and it involves an intermediate P_1^* which may be a triplet or a higher singlet state.

The ionization potential of pyrene is 7.55 eV in the gas phase.[32] Thus, photoionization requires more than just one photon of the exciting energy (3.68 eV). Although the ionization potential of pyrene adsorbed on alumina surfaces may be smaller than that in the gas phase, the linear relationship between the amount of cation radicals produced and the square of the laser pulse intensity suggests that the mechanism of photoionization is a two-photon process (see Figure 11). By contrast, the yield of the triplet increases linearly with the pulse energy as expected for a monophotonic process.

The decay profile of the cation radical exhibits a initial fast falloff followed by a slow decay which extends to a time scale of seconds. In the previous study,[12] the results from fluorescence study have indicated that there are a variety of adsorption sites for pyrene on the γ-alumina surface. These adsorption sites are the combination of the physisorption sites and the Lewis acid sites. Thus, the decay of the pyrene cation radical is described by the distribution of pyrene cation produced at different active sites. The interaction between the Lewis acid site and pyrene is most likely a charge-transfer type, which leads to cation radical. The cation radicals produced from pyrene adsorbed at the Lewis acid sites may decay faster because the radical ion pairs are in close proximity to each other. Conversely, the cation radicals that are produced on the physically adsorbed sites are well separated from the electrons by the hydroxyl groups and, accordingly, live longer. The combination of cation radicals produced at these different adsorption sites is well represented by a Gaussian distribution from which the average decay rate constant of the pyrene cation radical can be calculated. The increase in the rate of decay of P^+ with concentration of ferrocene enables a measurement of the diffusion quenching rate constant. The quenching rate constants of the pyrene cation radical by ferrocene are comparable with those for the pyrene triplet, supporting the idea of diffusional process by ferrocene along the surface, and not P^T or P^+. The effect of pretreatment temperature can be explained in the same way.

(32) (a) Birks, J. B.; Slifkin, M. A. *Nature* **1961**, *191*, 761. (b) Briegleb, G.; Czekalla, J. *Z. Elektrochem.* **1959**, *63*, 6.

Conclusion

Unlike silica surfaces, the alumina surface provides a variety of adsorption sites for adsorbed species: hydroxy physical adsorption sites and Lewis acid chemisorption sites. Organic molecules interact differently with these two adsorption sites. Diffusion process can be distinguished by the dynamic energy transfer from the triplet state of pyrene to coadsorbed ferrocene. Pretreatment of the surface at high temperature not only decreases the number of hydroxyl groups but also produces CUS cations which are known to be electron acceptors. A decrease in the bimolecular quenching rate constants on the surface at high T_a indicates a stronger interaction between adsorbed species and Lewis acid sites than on the physisorption sites. Hydration of the surfaces by coadsorbed water decreases the number of Lewis acid sites and enhances the dynamics of quenching. The bimolecular quenching rate constants obtained in the study are about 2 orders of magnitude smaller than those obtained on the silica surface, which indicates stronger bonding of organic molecules to the alumina surface. Formation of the cation radical of pyrene on alumina take places through a biphotonic mechanism which may involve the higher singlet excited states. Since the pyrene cation radicals are produced at different adsorption sites, the deactivation process of the cation radicals is explained in terms of diffusional recombination of the ion at different adsorption sites along the surface. Adsorbed ferrocene also quenches the cation radical in a dynamic fashion.

Acknowledgment. This work was supported by the Environmental Protection Agency via Grant EPA-R-815953-01-0.

Registry No. Pyrene, 129-00-0; pyrene radical ion, 34506-93-9; γ-alumina, 1344-28-1; ferrocene, 102-54-5.

Nuclear Magnetic Resonance Spectroscopic Study of Spin–Lattice Relaxation of Quadrupolar Nuclei in Zeolites

J. Haase, K. D. Park, K. Guo, H. K. C. Timken,† and Eric Oldfield*

Department of Chemistry, University of Illinois at Urbana-Champaign, 505 South Mathews Ave., Urbana, Illinois 61801 *(Received: November 20, 1990; In Final Form: April 1, 1991)*

We have obtained the temperature-dependent nuclear magnetic resonance spin–lattice relaxation times of several nonintegral spin quadrupolar nuclei (^{17}O, ^{23}Na, ^{27}Al, and ^{71}Ga) in a series of hydrated zeolites (NaA, NaX, NaY, NaGaY, and NH_4-ZSM-5) at 8.45 T. There is no correlation between T_1 and the static part of the electric field gradient, which gives rise to the observed nuclear quadrupole coupling constants (e^2qQ/h). In all cases, however, we find that relaxation is overwhelmingly dominated by modulation of the time-dependent electric field gradient at the nuclear site due to motion of water molecules and hydrated cations in the zeolite pores. The relaxation times are a function of Si/Al ratio as well as hydration. Our results provide estimates of the Sternheimer antishielding factors ($1 - \gamma_\infty$) in moderate agreement with generally accepted literature values and should be applicable to analysis of the relaxation behavior of other nonintegral spin quadrupolar nuclei in zeolites, e.g., ^7Li, ^{11}B, ^{39}K, ^{87}Rb, and ^{133}Cs.

Introduction

Recent developments in solid-state nuclear magnetic resonance (NMR) spectroscopy have permitted the determination of nuclear quadrupole coupling constants in a wide range of inorganic solids, such as zeolites,[1,2] so it is now natural to progress further by interpreting spin–spin[3] and spin–lattice relaxation in such systems. Preliminary results from this group[1,2,4] showed that ^{17}O spin–lattice relaxation in the zeolites Linde A and ZSM-5 was rather inefficient when compared with e.g. ^{27}Al NMR relaxation, even though static ^{17}O nuclear quadrupole coupling constants (e^2qQ/h) were

† Present address: Mobil Research and Development Corporation, Paulsboro Research Laboratory, Billingsport Road, Paulsboro, NJ 08066.

(1) Timken, H. K. C.; Janes, N.; Turner, G. L.; Gilson, J. P.; Welsh, L. B.; Oldfield, E. *J. Am. Chem. Soc.* **1986**, *108*, 7231.
(2) Timken, H. K. C.; Janes, N.; Turner, G. L.; Lambert, S. L.; Welsh, L. B.; Oldfield, E. *J. Am. Chem. Soc.* **1986**, *108*, 7326.
(3) Haase, J.; Oldfield, E. Submitted for publication.
(4) Timken, H. K. C. Ph.D. Thesis, University of Illinois at Urbana-Champaign, 1987, unpublished.

0022-3654/91/2095-6996$02.50/0

much larger than ^{27}Al e^2qQ/h values. Thus, phonon-based relaxation models could not be the cause of spin–lattice relaxation. More recently, Haase et al.[5] have shown that the short relaxation time of the ^{27}Al nucleus in some zeolite frameworks could be explained by the influence of moving water molecules and cations. Framework quadrupolar nuclei "feel" the fluctuating electric field gradient (efg) caused by the time-dependent motion of intracrystalline water and hydrated cations,[5] resulting in very efficient quadrupolar relaxation. In porous solids like zeolites, in which loosely bonded ions or adsorbed molecules may cause relaxation by modulating the efg at the site of the quadrupolar nucleus, these effects are much stronger than the electrical coupling of a quadrupolar nucleus to the phonon bath, as observed in more condensed materials, e.g. β-alumina.[6]

The model we develop for relaxation in zeolites is very simple: the total field gradient, eq^T, can be decomposed into a static part, eq^S, which dominates the observed nuclear quadrupole coupling constant, and a fluctuating part, $eq(t)$. The static quadrupole coupling constant can be written as

$$e^2qQ/h = eq^S eQ/h \tag{1}$$

while the fluctuating part, $eq(t)$, due to ion and water (dipole) motion, is exclusively responsible for spin–lattice relaxation (at least in hydrated samples in the approximate temperature range 25 → −100 °C and in the absence of large concentrations of paramagnetic centers). What is attractive about the model is that, for a given zeolite, e.g., a hypothetical (Li, Na, K) (B, Al, Ga–Y), *eq(t) is the same for each species present*, so as we show below, if the Sternheimer factor $(1 - \gamma_\infty)$ is known, then the T_1 values for all species can be related. For different zeolites, $eq(t)$ will of course vary and should be a function of e.g. hydration and Si/Al (or Ga, etc.) ratio.

We show below the applicability of this general model to ^{17}O, ^{23}Na, ^{27}Al, and ^{71}Ga relaxation in several zeolites. Good agreement between theory and experiment is obtained by using accepted Sternheimer antishielding factors. In addition, for a given zeolite, there is good agreement between the activation energies for relaxation for each nucleus present, as to be expected for the proposed model. When taken together with the results of spin-echo decay behavior on similar systems,[3] our results provide a relatively complete picture of spin dynamics in these materials.

Theoretical Background

Quadrupolar and Dipolar Coupling. For the nuclear magnetic resonance of quadrupolar nuclei ($I > 1/2$) with noninteger spins in a high magnetic field, the quadrupolar interaction, H_Q, is in general the major perturbation to the Zeeman interaction.[7] The central transition, $m = 1/2 \leftrightarrow -1/2$, is shifted only to second order in H_Q, whereas the satellite transitions are shifted to first order. For the NMR of powder zeolite samples with a quadrupolar frequency of more than ~200 kHz, the satellite transitions spread over a frequency range too wide to be observable by using conventional pulsed NMR instrumentation, due to the random microcrystallite orientations, and only the central transition is detected.

The frequency spread due to the orientational distribution in powder samples is usually too large to perform normal radio-frequency (rf) excitation and detection. However, although one only *observes* the central transition, the satellite transitions may still contribute to its intensity if they are excited by the rf pulse, represented by the Hamiltonian H_1. If the outer transitions become excited, the selection rule of H_1 ($\Delta m = \pm 1$) shows that these outer spins, by "moving" from $m = -3/2$ to $m = +3/2$, for example, pick up, at least partially, photons provided by H_1 and thus contribute to the observed intensity. In addition, for relaxation measurements, the number of excited spins in the outer transitions changes the relaxation behavior of the entire spin system. If only the central transition is excited, i.e., H_1 provides only photons close to the Larmor frequency, the probability that the spin system reaches a thermal equilibrium through the lattice-induced spin flipping ($H_Q(t)$, $\Delta m = \pm 1$ or ± 2) is higher than in the case of broad-band excitation, since for the latter case some of these flipping processes result in maintaining a zero-population difference between the central levels. This effect is well-known and may cause (for $I = 5/2$) up to a factor of 2 difference in measured spin–lattice relaxation times.[5,9] Since in most cases it is almost impossible to excite the entire spin system by a $\pi/2$ pulse, the best way to obtain reproducible relaxation rate behavior is to tune as close as possible to the central transition and measure the relaxation behavior of the system via the central transition.

In order to analyze our experimental results, we numerically solved the master equation of the population differences, N_m, of the Zeeman levels[7]

$$dN_m/dt = \sum_{m=-I}^{I} W_{nm}(N_n - N_m) \tag{2}$$

For the calculation of the transition probabilities, W_{nm}, we used the quadrupolar Hamiltonian given by the equation[8]

$$H_Q(t) = C_Q \sum_{k=-2}^{2} (-1)^k Q_k V_{-k}(t) \tag{3}$$

where

$$C_Q = \frac{eQ}{2I(2I-1)}, \quad Q_0 = \frac{1}{\sqrt{6}}\{3I_z^2 - I(I+1)\}$$

$$Q_{\pm 1} = \frac{1}{\sqrt{2}}\{I_{\pm 1}I_z + I_z I_{\pm 1}\}, \quad Q_{\pm 2} = \{I_{\pm 1}\}^2, \quad I_{\pm 1} = \mp\frac{I_\pm}{\sqrt{2}}$$

and

$$V_0 = (3/2)^{1/2}V_{zz}; \quad V_{\pm 1} = \mp(V_{zx} \pm iV_{zy}); \quad V_{\pm 2} = \tfrac{1}{2}(V_{xx} - V_{yy}) \pm iV_{xy}$$

This Hamiltonian is different from the static one insofar as fluctuations of the electric field gradient tensor components, $V_k(t)$, are given, we believe, by the Brownian motion of water molecules and cations. For this reason, we introduce the following correlation function for the components of the electrical field gradient tensor

$$\overline{V_k(t)\ V_{-k}(t+\tau)} = V_k^2 \exp(-|\tau|)/\tau_c) \tag{4}$$

where $V_k^2 = (eq)^2$ is assumed to be the same for $V_{\pm 1}$ and $V_{\pm 2}$ and τ_c is the correlation time, which should vary with temperature as

$$\tau_c = \tau_0 \exp(E_A/RT) \tag{5}$$

The transition probabilities then have the following form

$$W_{m,m\pm 1} = f_1(Q_{\pm 1})\frac{e^2Q^2}{\hbar^2}(eq)^2\frac{2\tau_c}{1 + (\omega_0\tau_c)^2} = f_1(Q_{\pm 1})W_1 \tag{6}$$

$$W_{m,m\pm 2} = f_2(Q_{\pm 2})\frac{e^2Q^2}{\hbar^2}(eq)^2\frac{2\tau_c}{1 + 4(\omega_0\tau_c)^2} = f_2(Q_{\pm 2})W_2 \tag{7}$$

where $f_{1,2}(Q_{\pm 1,2})$ are constants which depend on the spin quantum number, I.

It is known[5,9] that the relaxation process for an arbitrary ratio of the single- and double-quantum transitions, W_1 and W_2, may be multiexponential. However, for selective saturation of the central transition, the relaxation is well described by a single exponential. Figure 1 gives the theoretical dependences of the spin–lattice relaxation time, T_1, versus temperature, based on eqs 2–5, for the case of ideal broad-band saturation and selective

(5) Haase, J.; Pfeifer, H.; Oehme, W.; Klinowski, J. *Chem. Phys. Lett.* **1988**, *150*, 189.
(6) Villa, M.; Bjorkstam, J. L. *Phys. Rev. B* **1980**, *22*, 5033.
(7) Abragam, A. *Principles of Nuclear Magnetism*; Clarendon Press: Oxford, 1961.
(8) Haeberlen, U. *High Resolution NMR in Solids. Selective Averaging*; Academic Press: New York, 1976.
(9) Andrew, E. R.; Tunstall, D. P. *Proc. Phys. Soc. London* **1961**, *78*, 1.

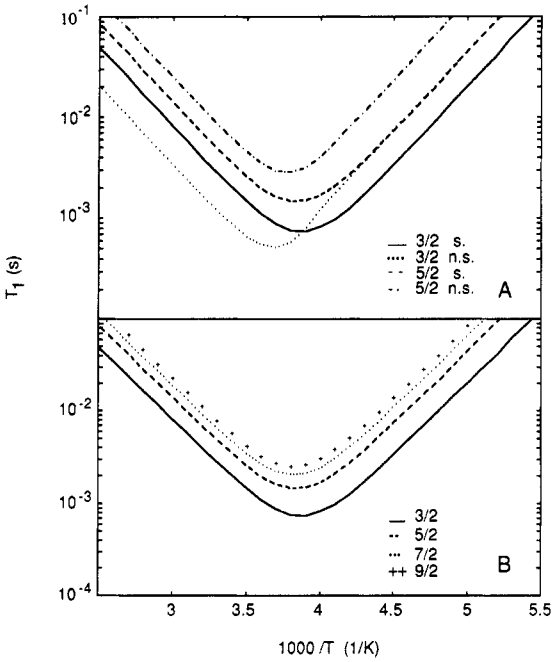

Figure 1. Theoretical temperature dependence of the spin–lattice relaxation time of nonintegral spin quadrupolar nuclei driven by classical correlation functions and activated processes, according to eqs 2–7, with the following constants: Larmor frequency 93.8 MHz; quadrupole moment $eQ = 0.15 \times 10^{-24}$ |e|·cm^2; $eq = 50$ V/nm^2; activation energy $E_a = 30$ kJ/mol; $\tau_0 = 1 \times 10^{-15}$. Only the spin quantum number, I, and the initial conditions vary: (A) —, $I = 3/2$, selective; ···, $I = 3/2$, nonselective; - - -, $I = 5/2$, selective; - · -, $I = 5/2$, nonselective. (B) Selective saturation: —, $I = 3/2$; - · -, $I = 5/2$; ···, $I = 7/2$; ++, $I = 9/2$.

saturation of the central transition only. For multiexponential relaxation, we define T_1 as the time for recovery of the magnetization to $1/e$ of its equilibrium value.

The observation that for selective saturation of the central transition the relaxation can be described by essentially a single-exponential term can be used to calculate the T_1 minimum by choosing the corresponding eigenvalue. This leads to $T_{1\min}$, the minimal T_1 value, of

$$T_{1\min} = k(I)\frac{\hbar^2\omega_0}{e^2Q^2(1-\gamma_\infty)^2(eq)^2} \tag{8}$$

where $k(I) = 3/2$, $10/3$, $21/4$, and $36/5$ for $I = 3/2$, $5/2$, $7/2$, and $9/2$, respectively. From Figure 1B, which shows the exact numerical calculations, we can examine the general applicability of eq 8. The somewhat smaller $T_{1\min}$ values for $I = 7/2$ and $I = 9/2$ in Figure 1B are due to the contribution of a faster decaying exponential term belonging to a different eigenvalue. In eq 8 we take into account the antishielding factor, $(1 - \gamma_\infty)$, which should cause an amplification of the relaxation process and varies with the particular nucleus under investigation.

Excitation Considerations. Excitation due to a radio-frequency pulse is described by the Fourier transform of the (generally) rectangular-shaped rf pulse. This provides excitation close to the carrier frequency, ω_0, described by $E(\Omega) = \omega_1 \sin(\Omega\tau/2)/\Omega$, where $\omega_1 = \|H_1\|/\hbar$ is the amplitude of the rf pulse and τ the pulse length. $\Omega = \omega_0 - \omega$ is the frequency difference between the carrier frequency and the frequency component, ω, of the pulse. For $\Omega\tau \rightarrow 0$, $E(\Omega)$ becomes $\omega_1\tau/2$, while for larger frequency offsets, the envelope of $E(\Omega)$ is inversely proportional to Ω only. This means that only the phase, and not the strength of excitation, depends on the pulse duration. In order to reduce any excitation of the outer levels, the pulse amplitude, represented by ω_1, thus has to be appropriately reduced. By reducing the rf power level, we always observe a sinusoidal dependence of the intensity of the central transition on the pulse length (at least up to a $3\pi/2$ pulse). By use of this "soft-pulse" method, the $\pi_s - \pi_s/2$ sequence, where "s" stands for solid and π_s means a pulse that inverts only the population of the central transition, we can determine T_1. We employed three different methods for measuring T_1: a hard-pulse saturating comb, a long soft-pulse saturation, and a soft-pulse ($\pi_s - \pi_s/2$) experiment. Although clearly the soft-pulse experiments are preferable, for historical reasons, several experiments were performed using the more conventional hard-pulse comb techniques. The two soft-pulse methods were shown to give the same relaxation times. The hard-pulse saturating-comb method gave somewhat longer T_1 values, as expected theoretically.

The excitation spectrum of a train of pulses (the Fourier transform of the comb) shows a train of spikes, the envelope of which is given by the Fourier transform of a single pulse used in the sequence. The width of a single spike in the frequency domain is inversely proportional to the number of pulses, and the excitation gap between two spikes is proportional to $1/T$, where T is the time between two pulses in the comb. To reach a more nonselective excitation by a comb, the time between pulses must permit some relaxation, because spin flipping between neighboring levels is forbidden (due to the strong quadrupolar interaction). In addition to these complications of a properly adjusted nonselective excitation, a multiexponential decay has to be expected, because only for the ideal case of $W_1 = W_2$ is the relaxation a single exponential. For these reasons, we have found that relaxation measurements employing the soft-pulse technique are more reliable and are thus recommended for future studies.

Experimental Section

Chemical Aspects. Preparation of ^{17}O-enriched zeolite NaA and the gallium analogue NaY are described elsewhere.[1,2,10] Zeolite NaX (13X) and NaY (SK30) were kindly provided by Dr. E. M. Flanigen (Union Carbide), and NH_4–ZSM-5 (Si/Al = 70:1) was kindly provided by Dr. K. Schmitt (Mobil). All samples were authenticated by means of X-ray powder diffractometry. The 52% relative humidity (52% rh) zeolites were prepared by equilibrating the samples over saturated $NaHSO_4$ in a closed container.[11] Zeolite NaY at 100% relative humidity (with H_2O) was prepared by equilibrating a sample over H_2O in a closed container, at ~24 °C. Zeolite NaY was ^{2}H exchanged by adding 0.6 g of ^2H_2O (99.9 atom % ^{2}H, Aldrich Chemical Co., Milwaukee, WI) to 0.5 g of zeolite, followed by equilibration overnight, at 45 °C. The sample was then dried at 100 °C for 4 h, followed by reequilibration over ^2H_2O in a sealed container, for several days. ^{17}O-enriched NaA was dehydrated under vacuum at room temperature for 24 h and then sealed in vacuo.

NMR Aspects. NMR spectra were obtained at 8.45 T with "home-built" NMR spectrometers, which consist of Oxford Instruments (Osney Mead, Oxford, U.K.) 8.45-T, 89-mm bore superconducting solenoid magnets, Nicolet Instrument Corp. (Madison, WI) Model 1280 computers for data acquisition, and Amplifier Research (Souderton, PA) Model 150LA or 200L amplifiers for final rf pulse generation. A "home-built" static probe equipped with glass or (for ^{27}Al and ^{23}Na NMR) quartz dewars was used. Sample temperatures ranged from 25 to −150 °C and were varied by use of a nitrogen gas flow. Spin–lattice relaxation times, T_1, were measured typically by using a saturating comb sequence (100, 3-μs pulses) to saturate the spin energy levels, for nonselective saturation, and either a single soft-pulse of 2-ms duration or a $\pi_s - \pi_s/2$ sequence for selective saturation. Chemical shifts are reported in ppm from external standards of tap water (^{17}O), 1 M NaCl (^{23}Na), 0.3 M $AlCl_3$ (^{27}Al), or 1 M $Ga(NO_3)_3$ (^{71}Ga). More positive values correspond to low-field, high-frequency, paramagnetic, or deshielded values (IUPAC δ scale).

Results and Discussion

We show in Figure 2 the static ^{17}O, ^{23}Na, ^{27}Al, and ^{71}Ga NMR spectra, at 8.45 T, of hydrated [^{17}O]NaA, NaA, NaY, and Ga-substituted NaY zeolites, respectively. There are several interesting features. First, the ^{17}O spectrum of NaA zeolite is clearly dominated by a second-order powder pattern line shape,[1,2] due

(10) Timken, H. K. C.; Oldfield, E. *J. Am. Chem. Soc.* **1987**, *109*, 7669.
(11) From Constant Humidity Table in: *CRC Handbook of Chemistry and Physics*, 62nd ed.; CRC Press: Boca Raton, FL, 1981; p E-44.

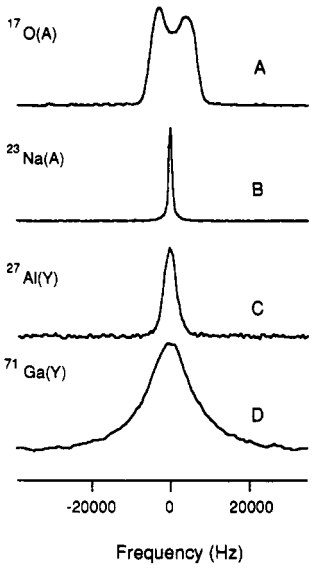

Figure 2. Representative ^{17}O, ^{23}Na, ^{27}Al, and ^{71}Ga static NMR spectra of various hydrated zeolite samples, at 8.45 T. (A) ^{17}O NMR of [^{17}O]NaA, 960 scans, 0.5-s recycle time, spin-echo pulse sequence, pulse widths of 2.4 and 4.8 μs (solid $\pi/2 - \pi$), 40-μs pulse separation, 500-Hz line broadening due to exponential multiplication. (B) ^{23}Na NMR of NaA, 400 scans, 0.3-s recycle time, 5 μs (10 μs, 90° solution) pulse excitation, 100-Hz line broadening due to exponential multiplication. (C) ^{27}Al NMR of NaY, 80 scans, 0.5 s recycle time, 3 μs (9 μs, 90° solution) pulse excitation, 100-Hz line broadening due to exponential multiplication. (D) ^{71}Ga NMR of Ga-analogue NaY, 1024 scans, 0.1-s recycle time, 17 μs (34 μs, 90° solution) pulse excitation, 1000-Hz line broadening due to exponential multiplication. The spectra are plotted on a hertz scale of arbitrary origin.

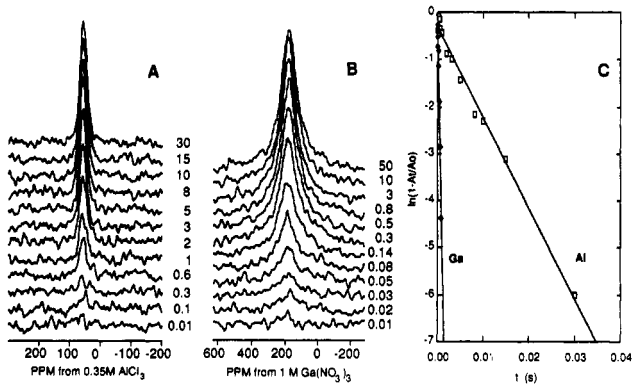

Figure 3. Partially relaxed ^{27}Al and ^{71}Ga Fourier transform NMR spectra of hydrated NaY and GaY zeolites, at 8.45 T, together with semilogarithmic magnetization recovery curves. (A) ^{27}Al spectra, 16 scans, 0.3-s recycle time, 24 μs (72 μs, 90° solution) pulse excitation, 100-Hz line broadening due to exponential multiplication. The τ values are given in ms. (B) ^{71}Ga NMR spectra, 1024 scans, 0.3-s recycle time, 6.5 μs (13 μs, 90° solution) pulse excitation, 1000-Hz line broadening due to exponential multiplication. The τ values given are in ms. (C) Magnetization decay curves for ^{27}Al (□) and ^{71}Ga (◆).

to a large static field gradient (eq^S). Because of the relatively low abundance and gyromagnetic ratio of ^{17}O, the additional broadening must be caused by heteronuclear dipolar interactions and is quite small. ^{23}Na and ^{27}Al resonances are, on the contrary, quite symmetric, reflecting much smaller static field gradients, due to higher symmetry and smaller antishielding factors and increased dipolar interactions. The ^{71}Ga spectrum is, by contrast, extremely broad. Given similar site symmetries and quadrupole moments for ^{27}Al and ^{71}Ga ($Q(^{27}Al) = 0.15 \times 10^{-28}$ m^2 and $Q(^{71}Ga) = 0.106 \times 10^{-28}$ m^2), the much broader and symmetric ^{71}Ga resonance can be explained by a stronger antishielding and, as we show below, a sizable T_1 contribution.

We show in Figure 3 representative ^{27}Al and ^{71}Ga saturating-comb recovery spectra of hydrated NaY and Ga-substituted

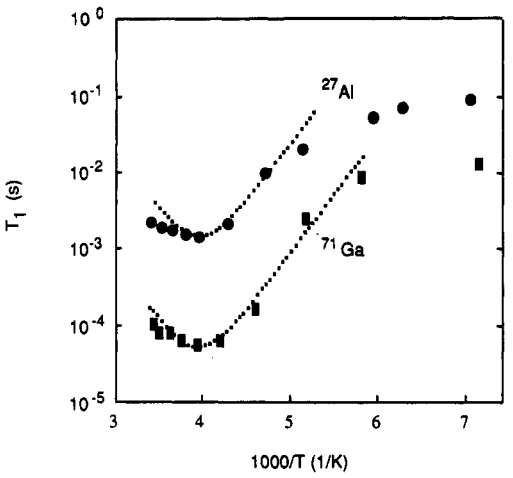

Figure 4. Temperature dependence of the 8.45-T spin–lattice relaxation times of ^{27}Al and ^{71}Ga nuclei in hydrated NaY (●) and GaY (■) zeolites (soft-pulse experiments), at 52% relative humidity. Dotted lines show theoretical fit to a single relaxation process.

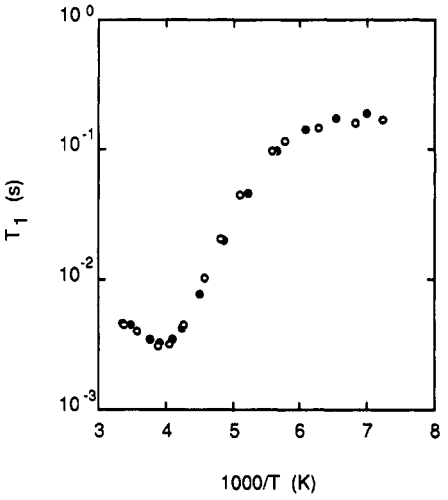

Figure 5. Temperature dependence of the spin–lattice relaxation times of ^{27}Al nuclei in NaY zeolites hydrated under H_2O (●) or ^2H_2O (○), at 8.45 T.

NaY zeolites, together with a semilogarithmic presentation of the magnetization recovery, ln $(1 - A_t/A_0)$, versus time. T_1 versus $1000/T$ results are shown in Figure 4. Figures 3 and 4 clearly indicate extremely rapid relaxation for Ga, which results in substantial lifetime line broadening. Figure 4 shows, at the minimum, that the T_1 of ^{71}Ga is 51 μs, while that of ^{27}Al is ~1.4 ms—some 27 times longer. While this difference in T_1 minima can be explained by several relaxation models, which in general will show T_{1min} inversely proportional to the quadrupolar coupling constant squared, the T_{1min} for the ^{17}O resonance—which has a much stronger quadrupolar coupling (cf. Figure 2)—clearly has a much longer T_1 value (T_{1min} = 5.7 ms) than either ^{27}Al or ^{71}Ga. In addition, the mobile ^{23}Na ion, with a very small quadrupole coupling constant, shows an even smaller T_{1min} than ^{27}Al (Table II). Fortunately, however, all of these results can be explained by using our model of a fluctuating efg, $eq(t)$, caused primarily by water motion, as described below.

Heteronuclear dipolar interactions with protons in water are expected to be unimportant in causing spin–lattice relaxation for most quadrupolar nuclei in zeolites, as exemplified by the ^{27}Al results shown in Figure 5 for the H_2O and ^2H_2O equilibrated NaY, as noted previously with NaX,[5] although heteronuclear dipolar interactions at low temperatures are a significant source of line broadening.[4] In order to estimate the influence of the dipole moment of the water molecules as contributors to the time-dependent modulation of the electric field gradients responsible for relaxation, we take as an example the experimental T_{1min} of ^{27}Al in NaY, 1.4 ms, and an antishielding factor $(1 - \gamma_\infty) = 3.59$ for

TABLE I: Estimated Ga Sternheimer Antishielding Factors for Ga-Analogue NaY Zeolite

$1 - \gamma_\infty$(Al)	ref	$(1/T_1)_{obs}$(Ga), s^{-1}	estd $(1 - \gamma_\infty$(Ga))
3.54	*a*	19600	14.3
3.59	*b*	19600	14.5
4.61	*c*	19600	18.6
3.91	*d*	19600	15.8[d]

[a] Sternheimer, R. M. *Phys. Rev.* **1966**, *146*, 140. [b] Das, T. P.; Bersohn, R. *Phys. Rev.* **1956**, *102*, 733. [c] Reference 13. [d] Average value of *a–c*.

the ^{27}Al nucleus (for which the variance in the literature is relatively small) and obtain by means of eq 8 an electric field gradient of $eq = 12.8$ V/(nm^2).

Now, the electric dipole moment p of a water molecule ($p = 6.14 \times 10^{-30}$ A s m) gives rise to an inhomogeneous (time dependent) electric field with a radial component of

$$E_r = \frac{1}{4\pi\epsilon_0}\frac{2p}{r^3} \tag{9}$$

or

$$V_r = \frac{-1}{4\pi\epsilon_0}\frac{6p}{r^4} \tag{10}$$

for the amount of the electric field gradient. Insertion of $eq = 12.8$ V/(nm^2) for V_r yields a radius $r = 0.40$ nm, consistent with the suggestion that water molecules are primarily responsible for the relaxation. (A typical Al–O distance in the zeolite A framework is 0.185 nm; the O–O distance between a framework oxygen and a hydrogen-bridged water molecule is about 0.275 nm.) We emphasize here that this time-dependent part of the electric field gradient, $eq(t)$, shows no correlation with the static part, e^2qQ/h. We now make the assumption that $eq(t)$ for ^{17}O, ^{23}Na, ^{27}Al, and ^{71}Ga are equal; i.e., the coupling of the nuclei with this quasi-classical "phonon bath" is given by the product of their quadrupolar moment and their antishielding response to a unique $eq(t)$ produced by the water molecules. With this assumption, we can fit all of the experimental results, as discussed previously, as shown in Table II.

If we compare the T_1 minima of ^{27}Al and ^{71}Ga in NaY zeolite (Figure 4), we can estimate by using an average literature value of $(1 - \gamma_\infty^{Al}) = 3.9$ (Table II) a $(1 - \gamma_\infty^{Ga}) = 19$, in moderate agreement with the average literature value[12,13] (cf. Table I) of $\approx$12, although we hasten to add that a factor of 2 in our T_{1min} prediction might more realistically take into account the total errors in determination of the T_1 minima and variances in literature $(1 - \gamma_\infty)$ values. The short T_{1min} values for Ga imply a substantial lifetime contribution to the line width, although quadrupolar effects are also important, and we have noted that substantial line narrowing at low temperatures (long ^{71}Ga T_1) is *not* achieved (data not shown), so that further work in this area appears desirable. Nevertheless, the T_{1min} value for ^{71}Ga is well predicted by use of the current model.

We now move on to consider the results on the framework anion, O^{2-}, as well as the nonframework cation, Na^+. Figure 6 shows typical T_1 versus $1000/T$ results for ^{17}O-labeled, hydrated, NaA, using a soft-pulse technique. Hard-pulse measurements were also performed, and the parameters deduced are shown in Table II. For the ^{23}Na resonance, hard-pulse experiments were done first to measure T_1 as a function of temperature. Soft-pulse excitation at a few temperatures was shown to yield the same T_1, within experimental error, indicating that even for weak excitation the satellites are still partially excited, due to motional averaging of the quadrupolar interaction. However, although for ^{23}Na the results for soft- and hard-pulse experiments are supposed to be

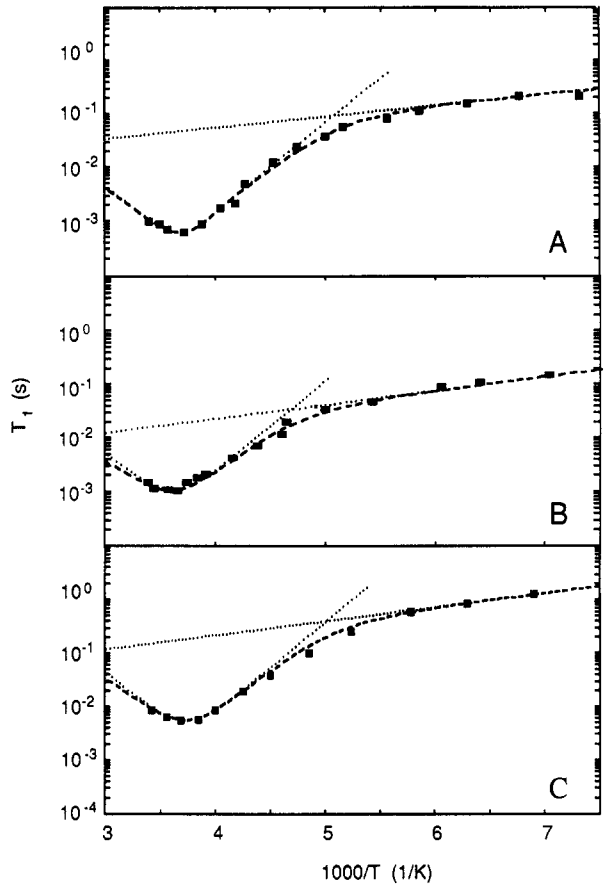

Figure 6. Temperature dependence of the spin–lattice relaxation times of (A) ^{23}Na, (B) ^{17}O, and (C) ^{27}Al nuclei in NaA zeolites (at 52% relative humidity), at 8.45 T (soft-pulse experiments), and theoretical fit (- - -) to two relaxation processes (···) by using the E_A, τ_0, and eq values given in Tables II and III.

the same, they were fit theoretically to both nonselective and selective saturation recovery data. We believe the selective (soft pulse) measurements are more accurate for ^{27}Al and ^{17}O, while for ^{23}Na, the nonselective ones are more appropriate, since nonselective excitation of the strongly quadrupolar broadened ^{27}Al and ^{17}O responances cannot be expected under our experimental conditions.

From these total electric field gradients, we can obtain the ratio of $(1 - \gamma_\infty)$ factors for ^{27}Al, ^{17}O, and ^{23}Na of 1:1.84:1.14. From ref 13, we obtain a ratio of 1:3.2:1.4, in moderate accord with the experimental observations. The difference between theory and experiment is greatest for ^{17}O, which may reflect more on the accuracy of the computed γ_∞ values for ^{17}O than on the model we have presented.

We now consider the E_A and τ_0 values deduced for the water motion. An activation energy of about 30 kJ/mol and $\tau_0 = 1 \times 10^{-15}$ s strongly suggest that rotation of the water molecules about their quasi-2-fold axis is responsible for the relaxation process.[14] For a given τ_0, the differences in the activation energy between the A, Y, and X zeolites may be significant, whereas τ_0 has a 50% variance. The fact that there is no dramatic change in the relaxation behavior at lower temperatures agrees well with the lack of a well-defined phase transition for H_2O in small clusters in zeolite pores, as noted previously by Pfeifer et al.[15]

We show in Figure 7 the ^{27}Al relaxation in NH_4–ZSM-5 and in Figure 8 the ^{27}Al and ^{17}O relaxation in $AlPO_4$-5 (hard-pulse measurements only). While the larger antishielding factor for ^{17}O again explains the differences between ^{27}Al and ^{17}O relaxation (cf. Table I), the activation energies of about 10 kJ/mol and τ_0

(12) Padhi, S. K.; Mohapatra, N. C. *Phys. Rev. B* **1984**, *29*, 5199. Sternheimer, R. M. *Phys. Rev.* **1963**, *130*, 1423. Burns, G.; Wikner, E. G. *Phys. Rev.* **1961**, *121*, 155. Wikner, E. G.; Das, T. P. *Phys. Rev.* **1958**, *109*, 360.

(13) Schmidt, P. C.; Sen, K. D.; Das, T. P.; Weiss, A. *Phys. Rev. B* **1980**, *22*, 4167.

(14) Larsson, K.; Tegenfeldt, J.; Kvick, Å. *J. Phys. Chem. Solids* **1989**, *50*, 107.

(15) Pfeifer, H.; Oehme, W.; Siegel, H. *Z. Phys. Chem. (Munich)* **1987**, *152*, 215.

TABLE II: Fitting Parameters for Temperature Dependence of Spin–Lattice Relaxation Time, T_1, in Various Systems

system	nucleus	$(1-\gamma_\infty)eq$,[a] V/nm²		T_{1min},[b] ms		T at T_{1min},[c] K		E_A,[d] kJ/mol		τ_0,[e] s	
		S[f]	NS[g]	S[f]	NS[g]	S[f]	NS[g]	S[f]	NS[g]	S[f]	NS[g]
NaY (52% rh)	^{27}Al	50		1.5		250		29.0		1×10^{-15}	
Ga-analogue NaY (52% rh)	^{71}Ga	290		0.051		250		29.0		1×10^{-15}	
NaA (52% rh)	^{27}Al	57	67	1.1	1.55	270	270	32.0	30.8	1×10^{-15}	1×10^{-15}
	^{17}O	105	110	5.7	10.1	270	270	32.4	32.0	1×10^{-15}	1×10^{-15}
	^{23}Na[h]	75	65	0.6	0.6	278	270	32.0	30.0	1×10^{-15}	1×10^{-15}
NaX (52% rh)	^{27}Al		57		2.2		250		28.4		1×10^{-15}
NH_4–ZSM-5 (52% rh)	^{27}Al		37		5.1		208		9		5×10^{-12}
$AlPO_4$-5 (52% rh)	^{27}Al		37		5.1				10.5		5×10^{-12}
	^{17}O		92		14.3		227		10.9		5×10^{-12}

[a] Total electric field gradient. [b] Magnitude of T_1 at the T_1 minimum. [c] Temperature of T_1 minimum. [d] Activation energy for the major relaxation process. [e] Preexponential correlation time factor. [f] Selective (soft-pulse) excitation. [g] Nonselective (hard pulse, saturating comb) excitation. [h] Experimental data set was fitted to both selective and nonselective excitation. Typical uncertainties from the fitting procedure alone are $\Delta V/V = 0.05$, $\Delta T/T = 0.05$, $\Delta E_A/E_A = 0.01$ for constant τ_0, $\Delta\tau_0/\tau_0 = 0.1$.

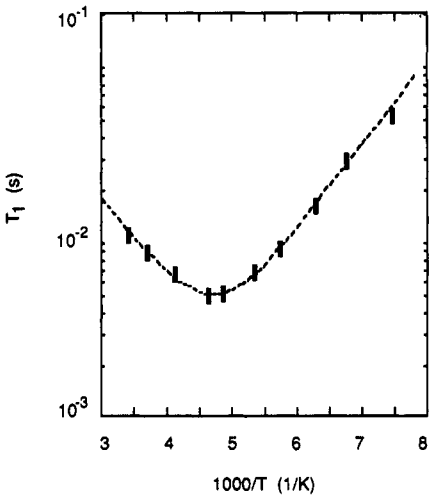

Figure 7. Temperature dependence of the ^{27}Al nuclear spin–lattice relaxation times of NH_4–ZSM-5, at 52% relative humidity and 8.45 T. Dashed line shows theoretical fit to a single relaxation process.

$= 5 \times 10^{-12}$ differ considerably from the faujasite type zeolites and are, we believe, connected with the more hydrophobic nature of the $AlPO_4$-5 and ZSM-5 materials—although at present we do not have a molecular interpretation of these observations.

Since the very high and very low temperature relaxation behavior of the faujasite type zeolites did not agree with the assumption of a single relaxation process, we have fitted the temperature-dependent relaxation behavior of these materials using a second, similarly activated process. The parameters found for the secondary process are given in Table III. While all results fit very well to an activation energy of 4–5 kJ/mol and $\tau_0 \approx (1-2) \times 10^{-7}$ s, the ratios between the total electric field gradients are different from those found for the main T_1 minimum. We note here that, although slow processes are known from the literature on glassy materials[16] and could be applicable to water in zeolite pores, the uncertainty of the fitting process, and the lack of experimental results at extremes of temperature, do not warrant further discussion. The influence of paramagnetic impurities at low temperatures, and the motion of the cations at high temperatures, seem likely candidates, and further work is under way in this area.

Conclusions

We believe the results we have presented above provide an excellent explanation of all of the relaxation data we have obtained to date on nonintegral spin quadrupolar nuclei in zeolites and could in suitable cases be useful for estimating Sternheimer antishielding factors. Our results are a logical extension of previous work on

(16) Avogadro, A.; Tabak, F.; Corti, M.; Borsa, F. *Phy. Rev. B* **1989**, *41*, 6137.

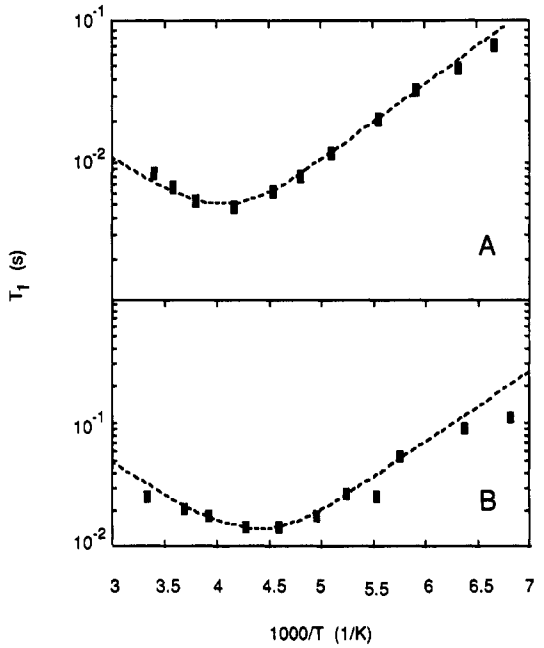

Figure 8. Temperature dependence of the (A) ^{27}Al and (B) ^{17}O nuclear spin–lattice relaxation times of $AlPO_4$-5, at 52% relative humidity and 8.45 T. Dashed line shows theoretical fits to a single relaxation process.

TABLE III: Fitting Parameters for the Second Relaxation Process in NaA and NaY Zeolites

	$(1-\gamma_\infty)eq$,[a] V/nm²		E_A,[b] kJ/mol		$10^7\tau_0$,[c] s	
	S[d]	NS[e]	S[d]	NS[e]	S[d]	NS[e]
NaA (52% rh)						
^{27}Al	280	310	5	4	1	2
^{17}O	270	340	5	5	1	1
^{23}Na		200		4		1
NaY (52% rh)						
^{27}Al	300		4		2	
^{71}Ga	800		4		2	

[a] Total electric field gradient. [b] Activation energy (for this second, minor relaxation process). [c] Preexponential correlation time factor. [d] Selective (soft-pulse excitation). [e] Nonselective (hard pulse, saturating comb) excitation.

Al NMR in NaA and NaX,[5] and the multinuclear results presented here confirm the basic correctness of the model of a water-dominated fluctuating electric field gradient, $eq(t)$. In particular, our results provide a convincing explanation of the lack of any correlation between e^2qQ/h and T_1, which would be expected for phonon models. Although not yet proven, it seems likely that *one* T_1 experiment on a given zeolite could predict, with reasonable accuracy, the e.g. Li, Na, K, Rb, and Cs nonframework or B, O, Al, and Ga framework nuclear spin–lattice relaxation

behavior, at least when the quadrupolar interaction dominates. Further work to check this hypothesis, to investigate the effects of di- and trivalent cations, to investigate framework substitutions in AlPO-*n* materials, to investigate in more detail the effects of Si/Al ratio and zeolite hydration, and to investigate relaxation over a much wider temperature range is in progress.

Acknowledgment. This work was supported by the Solid State Chemistry Program of the U.S. National Science Foundation (Grant DMR 88-14789).

Registry No. ^{17}O, 13968-48-4; Na, 7440-23-5; Al, 7429-90-5; ^{71}Ga, 14391-03-8.

Correlation of Electron-Transfer Rates with the Surface Density of States of Native and Anodically Grown Oxide Films on Titanium

Norberto Casillas, Shelly R. Snyder, William H. Smyrl, and Henry S. White*

Department of Chemical Engineering and Materials Science, University of Minnesota, Minneapolis, Minnesota 55455 *(Received: November 26, 1990)*

We report tunneling spectroscopy (TS) and surface density of states (SDOS) plots ($(dI/dV)/(I/V)$ vs V) for native and anodically grown titanium dioxide (TiO_2) films on polycrystalline Ti. The results are compared to data obtained by using single-crystal TiO_2 ((001) and (110) surface orientations). SDOS plots for anodically grown TiO_2 films (160 Å thick) and single-crystal TiO_2 show a large bandgap region (~2 eV) with a low state density separating the conduction and valence band edges. The similarity in the distribution of SDOS for anodically grown TiO_2 films and single-crystal TiO_2 indicates that the anodically grown film has a well-ordered rutile structure. In contrast, SDOS plots obtained on native TiO_2 films show a nearly constant density of states over a 5-eV range and a ~20–50-fold increase in state density at energies corresponding to the bandgap region of anodically grown films and single-crystal TiO_2. Electron-transfer rates for the oxidation of ferrocene in acetonitrile at native and anodically grown TiO_2 films are reported and correlated with the measured SDOS of these materials.

Introduction

The chemical stability of titanium is due to a native oxide film that spontaneously forms on the surface of the metal in air and in most oxygen-containing environments, eq 1. The equilibrium

$$Ti + O_2 \rightarrow TiO_2 \quad (1)$$

of reaction 1 lies far to the right ($\Delta G = -212.6$ kcal/mol),[1] and the resulting oxide film (~20 Å)[2] reduces the rate of metal oxidation to a negligible value in ambient environments. Localized breakdown of the native film occurs in chemically aggressive environments (e.g., aqueous Br^- solutions) resulting in rapid local dissolution of the metal substrate. Although the mechanisms for oxide breakdown and resulting local metal dissolution are poorly understood for Ti and most other metals (e.g., Fe, Cu), it is frequently assumed that electric-field-assisted electron- and/or ion-transfer reactions on the oxide film are involved. The chemical and electronic properties of the native film that control interfacial charge transfer are, thus, of both fundamental and technological interest.

The properties of both native and thicker, anodically grown TiO_2 films have been studied by using photoelectrochemical microscopy (PEM).[3-5] In the PEM experiment, the photocurrent response of a TiO_2 film is measured in an electrolyte solution as a laser is rastered across the surface. The results of such experiments have been correlated with differences in film crystallinity and oxide orientation as measured by X-ray and electron diffraction. While photoelectrochemical microscopy provides information concerning the electronic and structural properties of the oxide layer with a lateral resolution of several microns, the development of more direct methods of probing the surface electronic properties with higher lateral resolution is required to develop atomic-level mechanisms of charge-transfer reactions on oxide films.

Prior to this report, a number of authors have used scanning tunneling microscopy[6] (STM) and tunneling spectroscopy (TS)[7] to characterize the topography and electronic properties of TiO_2 surfaces in air and aqueous environments.[8-14] Recently, Fan and Bard have reported atomically resolved STM images of doped, single crystal TiO_2 (001) in air.[12] In addition, these authors reported TS data from which they obtained a semiconductor band gap of ~3.0 eV, in agreement with the bulk value for rutile TiO_2. Gilbert and Kennedy have also reported TS data taken in air on doped single-crystal TiO_2 (001).[13] Sakamaki et al. studied surfaces of the highly doped and hydroxylated TiO_2 (110) surface. Their findings suggest a reduction in the bandgap of TiO_2 relative to the accepted bulk value, a difference attributed to the existence of chemisorbed OH^- groups.[14]

In this paper, we report a detailed comparison of TS results obtained on native TiO_2 films, anodically grown TiO_2 films, and the (001) and (110) surface orientations of single-crystal rutile TiO_2 previously reported by the above-mentioned researchers. We observe that the native oxide of Ti has a significantly higher density of electronic states at energies corresponding to the bandgap regions of single-crystal rutile and anodically grown TiO_2 films. In the last section of this report, we describe electron-transfer rate measurements for the oxidation of a reversible redox species (ferrocene) on native and anodically grown films. We show that

(1) Weast, R. C.; Astle, M. J. *Handbook of Chemistry and Physics*, 63rd ed.; CRC Press, Inc.: Boca Raton, FL, 1982.
(2) (a) Aladjem, A. *J. Mater. Sci.* **1973**, *8*, 688. (b) Lausmaa, J.; Kasemo, B. *Appl. Surf. Sci.* **1990**, *44*, 133.
(3) Kozlowski, M. R.; Tyler, P. S.; Smyrl, W. H.; Atanasoski, R. T. *Surf. Sci.* **1988**, *194*, 505.
(4) Tyler, P. S.; Kozlowski, M. R.; Smyrl, W. H.; Atanasoski, R. T. *J. Electroanal. Chem.* **1987**, *237*, 295.
(5) Leitner, K.; Schultze, J. W.; Stimming, U. *J. Electrochem. Soc.* **1986**, *133*, 1561.
(6) Binnig, G.; Rohrer, H. *IBM J. Res. Dev.* **1986**, *30*, 355.
(7) Stroncio, J. A.; Feenstra, R. M.; Newns, D. M.; Fein, A. P. *J. Vac. Sci. Technol.* **1988**, *A6*, 499.
(8) Miranda, R.; Garcia, N.; Baro, A. M.; Garcia, R.; Peña, J. L.; Rohrer, H. *Appl. Phys. Lett.* **1985**, *47*, 367.
(9) Morita, S.; Okada, T.; Ishigame, Y.; Sato, C.; Mikoshiba, N. *Jpn. J. Appl. Phys.* **1986**, *25*, L516.
(10) Gilbert, S. E.; Kennedy, J. H. *J. Electrochem. Soc.* **1988**, *135*, 2385.
(11) Itaya, K.; Tomita, E. *Chem. Lett.* **1989**, 285.
(12) Fan, F.-R. F.; Bard, A. J. *J. Phys. Chem.* **1990**, *94*, 3761.
(13) Gilbert, S. E.; Kennedy, J. H. *Surf. Sci. Lett.* **1990**, *225*, L1.
(14) Sakamaki, K.; Itoh, K.; Fujishima, A.; Gohshi, Y. *J. Vac. Sci. Technol. A* **1990**, *8*(1), 614.

0022-3654/91/2095-7002$02.50/0